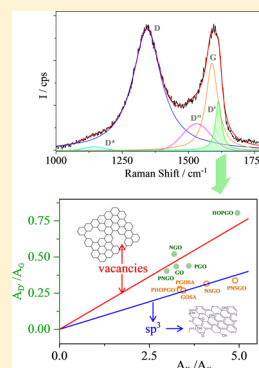


Evolution of the Raman Spectrum with the Chemical Composition of Graphene Oxide

David López-Díaz,[†] Marta López Holgado,[†] José L. García-Fierro,[‡] and M. Mercedes Velázquez^{*,†}[†]Departamento de Química Física, Facultad de Ciencias Químicas, Universidad de Salamanca, E37008 Salamanca, Spain[‡]Instituto de Catálisis y Petroleoquímica, CSIC, 28049 Cantoblanco, Madrid Spain

Supporting Information

ABSTRACT: Raman spectra of graphene oxides (GOs) with different chemical compositions and synthesized by oxidation of distinct starting materials were analyzed to relate the spectral features to structural properties. The chemical compositions of different graphene oxides were determined by X-ray photoelectron spectroscopy (XPS), and nanoplatelets were characterized by zeta potential (ζ) and dynamic light scattering (DLS) measurements. The results indicated that the chemical composition, size, and superficial charge of the nanoplatelets depend on the starting material. We found five reported bands (D, D', G, D'', and D*) in the first-order Raman spectrum and three bands (2D, D + D', and 2D') in the second-order Raman spectrum that successfully interpret the Raman spectra between 1000 and 3500 cm^{-1} . Analysis of the bands allowed linear correlations to be found between the maximum positions of the 2D and D + D' bands and between the relative intensities of the D and G bands (I_D/I_G) and the Csp² percentage. Moreover, our results demonstrate that the relative intensities of the D' and D bands are in excellent agreement with the theoretical correlations and allow the type of defects produced during oxidation, namely, vacancies or sp³ hybridation, to be related to the size of the graphene oxide sheets.



1. INTRODUCTION

Graphene is a two-dimensional (2D) material consisting of a monolayer of sp²-hybridized carbon atoms arranged in a honeycomb lattice. Because of its unique mechanical, thermal, and electric properties, graphene has attracted increased interest and has been proposed as a component of transparent conducting electrodes, transistors, and supercapacitors.^{1,2} The excellent properties of graphene are closely linked to the absence of chemical and structural defects in the network and stacked layers.

Graphene has been synthesized by both bottom-up and top-down methodologies.³ Bottom-up methods involve synthesizing graphene from carbonaceous gas sources. Some examples of bottom-up methods include chemical vapor deposition⁴ and epitaxial growth on silicon carbide.⁵ In contrast, top-down methods consist of separating the stacked sheets of graphite by different methodologies including solvent-based exfoliation,⁶ exfoliation of graphite intercalated compounds (GICs),⁷ and exfoliation of graphite into graphene oxide (GO) followed by reduction of graphene oxide.^{8–12} Because of the need to find large-scale graphene production methods, graphene oxide has been identified as one of the most important graphene derivatives. However, graphene oxide reduction does not allow for the removal of all chemical and structural defects; consequently, graphene oxide becomes an insulating material. However, despite this important limitation, the properties of graphene oxide can be tuned through the introduction or removal of defects, which can be structural or due to attached molecules, such as polymers, or nanoparticles. These new materials are potential candidates for the fabrication of polymer

composites,¹³ gas sensors,¹⁴ or photovoltaic applications;^{15,16} therefore, defect identification and quantification is a crucial issue.

Raman spectroscopy is a powerful technique for detecting defects because its phonon modes provide explicit information about changes in the layer structure produced by structural or chemical defects. Thus, studies carried out by the Ferrari^{17–19} and Dresselhaus^{20–24} groups have demonstrated that the most prominent features in the Raman spectrum of monolayer graphene are the G band centered at 1582 cm^{-1} and the G' (2D) band at about 2700 cm^{-1} . These peaks always satisfy the Raman selection rules.²¹ However, when the periodic lattice of graphene is broken by defects, two new Raman-forbidden bands appear; they are referred to as the D and D' bands and are centered at 1350 and 1626 cm^{-1} , respectively.²⁵ These bands are activated by single-phonon intervalley and intravalley scattering processes, respectively. Simultaneously, the 2D band reduces in intensity, and a broad feature from 2300 to 3100 cm^{-1} appears. This feature has been assigned to 2D' and combination bands.^{17,26,27} The presence or absence of these bands and their relative positions, intensities, and shapes provide information about the existence and nature of defects in graphene derivatives.

In the particular case of the Raman spectrum of graphene oxide, a great variety of results can be found in the literature. For example, several reports have shown changes in the

Received: June 26, 2017

Revised: August 18, 2017

Published: August 25, 2017

position and width of the G band attributed to high defect concentrations produced by the oxidation process. These changes are often accompanied by the appearance of new bands related to different classes of defects such as single and multiple vacancies, Stone–Wales defects, and rings with C–O bonds.^{28–31} Other works have reported Raman spectra of graphene oxides in which the D and G bands are equally intense and the 2D band presents a low intensity. In fact, in many works, the 2D band is not even mentioned. On the other hand, *ab initio*³² and density functional theory (DFT)³³ calculations have been used to simulate the Raman spectra of graphene oxides of different chemical compositions. These calculations have demonstrated that the intensity and width of the G band and the appearance of new bands in the GO Raman spectrum depend on the local atomic configuration. In light of these facts, the interpretation of the GO Raman spectrum requires a systematic study of the effects of the functional groups on graphene oxide Raman spectrum. For example, a good correlation between the width of the D band and the sp^2 content has been reported for reduced graphene oxides (RGOs).³¹ In that work, RGO materials were obtained by chemical reduction of GO for different times, followed of thermal annealing.³¹ On the other hand, in a previous work,³⁴ we demonstrated that the Raman spectra of graphene oxides synthesized from GANF carbon nanofibers and thermally reduced at temperatures ranging between 100 and 800 °C present D, D', G, D'', and D* Raman bands. Our results also demonstrated that the peak positions of the D'' and D* bands exhibit a pronounced dependence of the oxygen content determined by elementary analysis. Moreover, the $I_{D''}/I_G$ intensity ratio and the width of the D'' band decrease when the crystallinity of the sheets increases, whereas the I_{D^*}/I_G ratio decreases when the number of sp^3 bonds in the sheets decreases. It is interesting to note that, in that work, we were interested in maintaining a certain degree of structural order inside the network because we were interested in studying the effect of the chemical composition of GO on the Raman spectrum, minimizing heterogeneity effects. Therefore, we selected GANF carbon nanofibers as the starting material because they produce GO sheets that are more homogeneous than those obtained by graphite oxidation.^{35,36} However, in this work, we are interested in extending the investigation to other graphene oxides; therefore, in the current work, we synthesized GO by the oxidation of five starting materials: three different types of graphite and both graphitized and nongraphitized commercial carbon nanofibers. The graphene oxides thus obtained were further purified by alkaline washing to eliminate oxidative impurities, resulting graphene oxides with different chemical compositions. Using this strategy, we obtained 10 different graphene oxides, which allowed us to correlate the Raman spectrum of graphene oxide with its chemical composition and structural defects.

2. EXPERIMENTAL SECTION

2.1. Materials. To obtain graphene oxides with different chemical compositions, we oxidized distinct materials. The starting materials selected were natural graphite flakes (99.02% fixed C) from Qingdao Super Graphite Co., Ltd.; graphite flakes (+100 mesh) and highly oriented pyrolytic graphite (HOPG) provided by Sigma-Aldrich (St. Louis, MO); and GANF helical-ribbon carbon nanofibers (graphitized and nongraphitized) provided by Carbon Advanced Materials, Grupo Antolín (Burgos, Spain). Commercial GANF carbon

nanofibers are produced by chemical vapor deposition (CVD) using the floating catalyst method.³⁵ NaNO_3 (99%), H_2SO_4 [98% (w/w)], KMnO_4 (>99%), H_2O_2 [30% (w/w)], NaOH, and HCl (35%) were provided by Sigma-Aldrich and were used without further purification. Millipore Ultrapure water prepared using a combination of RiOs and Milli-Q systems from Millipore was used to prepare solutions and reaction mixtures. The solid substrates were silicon (100) wafers with a 300-nm dry thermal SiO_2 thin film to enhance the optical contrast of the flakes under white-light illumination.³⁷

We also purified graphene oxide materials by alkaline washing.^{12,38} The purification procedure eliminates highly oxidized impurities,^{12,38} providing graphene oxides with lower oxidation degrees than the nonpurified samples.^{12,35,38–40} Using these strategies, we obtain graphene oxides with different oxidation degrees and different percentages and types of O-containing groups attached at the basal plane. A list of acronyms corresponding to the various graphene oxides is provided at the end of the main text of the article. A previously reported modified Hummers method^{10,35} was used to obtain graphene oxides from different starting materials, and the purification procedure was reported by Rourke et al.³⁸

2.2. Experimental Methods. X-ray photoelectron spectra of powder samples were recorded in a VG Escalab 200R spectrometer (Fisons Instruments, Parkton, MD) equipped with a excitation source of Mg $K\alpha$ ($h\nu = 1253.6$ eV) radiation and a hemispherical electron analyzer. High-resolution spectra were recorded working at a 20 eV analyzer pass energy. The residual pressure in the analysis chamber was maintained below 4×10^{-7} Pa during data acquisition.

Zeta potential measurements were carried out by means of the laser Doppler electrophoresis technique using a Zetasizer Nano ZS device (Malvern Instruments, Malvern, U.K.). The electrophoretic mobility, μ_e , was measured at 20.0 °C using a DTS 1060C disposable cell and was further converted into zeta potential, ζ , using the Smoluchowski relationship,⁴¹ $\zeta = \eta\mu_e/\epsilon$, where η and ϵ are the absolute viscosity and permittivity of water at 20.0 °C, respectively. The solution concentration was 0.12 mg mL⁻¹.

DLS experiments were performed in a Zetasizer Nano ZS device (Malvern Instruments, Malvern, U.K.) at 20.0 °C, and the intensity autocorrelation function was obtained at 13 °C and transformed into electric field autocorrelation functions according to the Siegert relationship, $g^2(q;\tau) = 1 + [g^1(q;\tau)]^2$, where $g^2(q;\tau)$ and $g^1(q;\tau)$ are the second-order and first-order autocorrelation functions, respectively, and β represents a correction factor that depends on the geometry and alignment of the laser beam in the light scattering setup.⁴² We used DLS measurements to estimate the sheet sizes because we previously demonstrated that the values estimated using this methodology agree acceptably with the size values estimated from scanning electron microscopy (SEM) images.³⁹

Raman scattering measurements were carried out at room temperature with a LabRAM HR Evolution micro-Raman spectrometer (Horiba Jobin-Yvon). The spectrometer is equipped with a solid-state laser operating at 532 nm and a 100× objective (laser spot size $\approx 1 \mu\text{m}^2$). Accurate calibration was carried out by checking the Rayleigh band and Si band at 0 and 520.7 cm^{-1} , respectively. To obtain the Raman spectra of the various materials, the graphene oxides were deposited onto silicon wafers by the drop-casting method. The sample area was scanned with a spatial resolution of approximately 0.5 μm ; the acquisition time was 3 s at each point, and five spectra were

accumulated. The laser excitation power was kept below 1 mW to avoid laser-induced heating. Each Raman spectrum was recorded in at least four different zones for three representative flakes for each material; accordingly, the spectra presented in the figures are averages of all of these measurements. Raman-scattered light was analyzed using a diffraction grating (1800 lines mm^{-1}) and a CCD camera. The spectral resolution of the reported spectra was close to 2 cm^{-1} .

The first-order Raman spectra were fitted to sums of functions using Origin 8.0 software. Lorentzian, Gaussian, pseudo-Voigt, and Breit–Wigner–Fano functions are widely used to fit the Raman spectra of carbonaceous and graphene-based materials, with many well-established rules for choosing one particular function.^{17,43–46} During the analysis, it was found that Gaussian functions better fit D^* and D'' bands, whereas the best fits for D, G, and D' bands were achieved using pseudo-Voigt functions. This behavior agrees very well with that observed for graphene oxides reduced by thermal annealing.³⁴ The second-order spectrum was split into four Lorentzian contributions.²⁸

3. RESULTS AND DISCUSSION

3.1. Structural Characterization of Graphene Oxide.

Before the Raman spectra of the graphene oxides were recorded, the chemical compositions were calculated from the analysis of the X-ray photoelectron spectra. Illustrative examples of the C 1s core-level spectra for purified (PNSGO) and nonpurified (NSGO) graphene oxide obtained by the oxidation of GANF nanofibers are presented in Figure 1. The rest of the XPS spectra are collected in Figure S1 of section 1 of the Supporting Information.

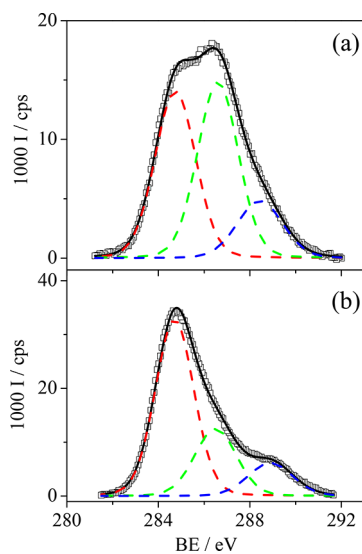


Figure 1. X-ray photoelectron spectra of C 1s core levels of (a) NSGO and (b) PNSGO. Squares are experimental data, dashed lines represent the functions into which we split the spectrum, and solid lines are fits to the data.

In each case, the C 1s core-level spectrum is an asymmetric band that can be fitted by three components centered at 284.8, 286.4, and 287.9 eV. It is well-established that these peaks are assigned to aromatic carbon bonds (284.8 eV), to C–O bonds corresponding to alcohol or epoxy groups (286.4 eV), and to COO^- groups (287.9 eV).⁴⁷ The atomic percentages of the different groups were calculated from the areas of these peaks.

Table 1 contains a summary of the band positions, percentages of different species, and C/O and $\text{Csp}^2/\text{Csp}^3$ ratios.

Table 1. Values of Binding Energies, Percentages of Different Groups, C/O Surface Atomic Ratios, and $\text{Csp}^2/\text{Csp}^3$ Ratios for Different Graphene Oxides Obtained from XPS Measurements

sample	bond	maximum (eV)	Csp^2 content (%)	C/O	$\text{Csp}^2/\text{Csp}^3$
GO ^a	C=C	284.8	51 ± 3	1.6	1.04
	C–O	286.4	42 ± 2		
	COO^-	287.9	7 ± 0.4		
PGO ^a	C=C	284.8	72 ± 4	4.3	2.6
	C–O	286.4	20 ± 1		
	COO^-	288.2	8.0 ± 0.4		
GOSA	C=C	284.8	49 ± 2	1.92	0.96
	C–O	286.6	37 ± 2		
	COO^-	288.5	14 ± 1		
PGOSA	C=C	284.8	64 ± 3	3.82	1.56
	C–O	286.5	18 ± 1		
	COO^-	288.6	18.0 ± 0.9		
HOPGO	C=C	284.8	58 ± 3	1.50	0.93
	C–O	286.4	29 ± 1		
	COO^-	288.4	12 ± 1		
PHOPGO	C=C	284.8	60 ± 3	3.63	1.5
	C–O	286.4	27 ± 1		
	COO^-	287.7	13.0 ± 0.7		
NGO ^b	C=C	284.8	60 ± 3	1.6	1.5
	C–O	286.4	26 ± 1		
	COO^-	287.9	14.0 ± 0.7		
PNGO ^b	C=C	284.8	72 ± 4	2.63	2.6
	C–O	286.4	23 ± 1		
	COO^-	287.9	5.0 ± 0.3		
NSGO	C=C	284.8	42 ± 2	1.85	0.75
	C–O	286.4	44 ± 2		
	COO^-	288.4	14 ± 1		
PNSGO	C=C	284.8	60 ± 3	3.57	1.5
	C–O	286.4	26 ± 1		
	COO^-	288.4	14 ± 1		

^aData taken from ref 38. ^bData taken from ref 35.

The data in Table 1 show significant differences between the chemical compositions of purified and nonpurified graphene oxides. Thus, the purified oxides contain higher C/O and $\text{Csp}^2/\text{Csp}^3$ ratios than the nonpurified ones. This fact was previously reported^{12,35,38–40} and was attributed to the elimination of highly oxidized organic fragments strongly adsorbed on graphitic sheets due to alkaline washing. An exception to this behavior is the case of graphene oxides synthesized from highly oriented pyrolytic graphite, for which the chemical composition remained almost unaltered by the purification process. The results in Table 1 also show that the percentages of alcohol and epoxy groups localized at the basal plane decreased after purification and that the effect depended on the nature of the starting material. Finally, the percentage of COOH groups did not seem to exhibit a clear dependence on the purification process. However, in previous works, we reported some dependence between the percentage of carboxylic acids and the nanoplatelet size.^{35,39} To confirm this relationship, we have plotted in Figure 2a the apparent diameter determined from DLS against the percentage of COOH groups determined from XPS spectra. On the other hand, because the carboxylic groups

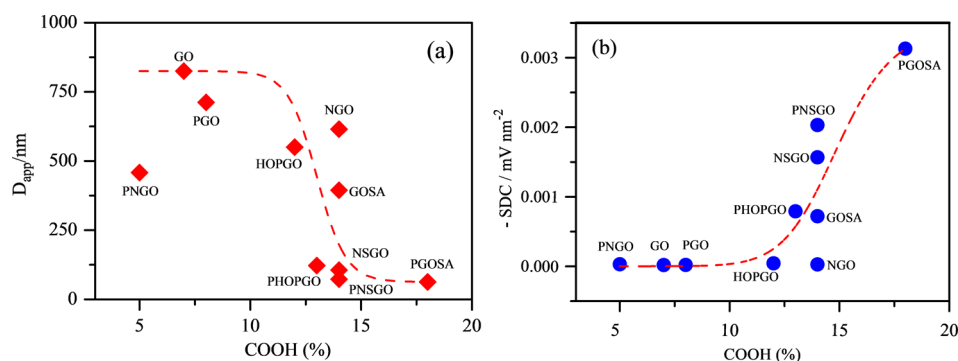


Figure 2. Variations in (a) the apparent hydrodynamic diameter of nanoplatelets estimated from DLS and (b) the superficial charge density values as functions of the percentage of COOH groups attached to the basal plane of the graphene oxides. Dotted lines are just visual guides.

are ionized in aqueous solutions,⁴⁸ one expects that the chemical composition could modify the superficial charge density (SCD). To analyze this issue, the superficial charge density values were plotted against the percentage of carboxylic groups (see Figure 2b). For each material, the SCD was estimated as the ratio between the zeta potential and the nanoplatelet area calculated as the area of a circle whose radius was that obtained by DLS measurements. It is necessary to consider that the apparent hydrodynamic radius obtained by DLS measurements is just a raw estimation because our equipment uses the Stokes model, which considers a spherical geometry that the graphene sheets lack. However, our previous results confirmed that the nanoplatelet radius obtained from DLS adequately agrees with the size values estimated from SEM images;³⁹ consequently, we used the DLS measurements to estimate the nanoplatelet sizes. According to our previous results, the autocorrelation functions of graphene oxides present a nonexponential behavior that, when analyzed using regularized inverse Laplace transforms, yield asymmetric and broad complex distribution functions indicative of populations of different size; see more details in Figure S2 of section 1 of the Supporting Information. Therefore, the apparent hydrodynamic diameter values plotted in Figure 2a correspond to the maximum of each distribution function.

The results in Figure 2a show that the nanoplatelet size correlates with the percentage of carboxylic acid groups attached to the basal plane. According to our results, the largest sheets present lower percentages of COOH groups than the smallest ones. This behavior was previously reported³⁹ and was attributed to the oxidation process at the edge of platelets: Because carboxylic groups predominate at the nanoplatelet edges, the smallest sheets present higher percentages of carboxylic acids than the larger sheets. Concerning the superficial charge density value, Figure 2b shows that it increased when the percentage of carboxylic acid increased. The effect was more pronounced when the percentage of carboxylic groups reached a value of about 12–14%. These results seem to indicate that the carboxylic groups mainly provide the electrical charge to the graphene oxide flakes and that the SDC increases above a given carboxylic percentage value (14%) that corresponds to the smallest sheets.

3.2. Raman Spectra of Graphene Oxides. After chemical characterization, the Raman spectra of the graphene oxides deposited onto silicon wafers were recorded (see Figure 3a). As can be seen in Figure 3a, all of the spectra present D and G peaks centered at ~ 1350 and ~ 1585 cm^{-1} , respectively, and a second-order band centered at ~ 2900 cm^{-1} . The Raman

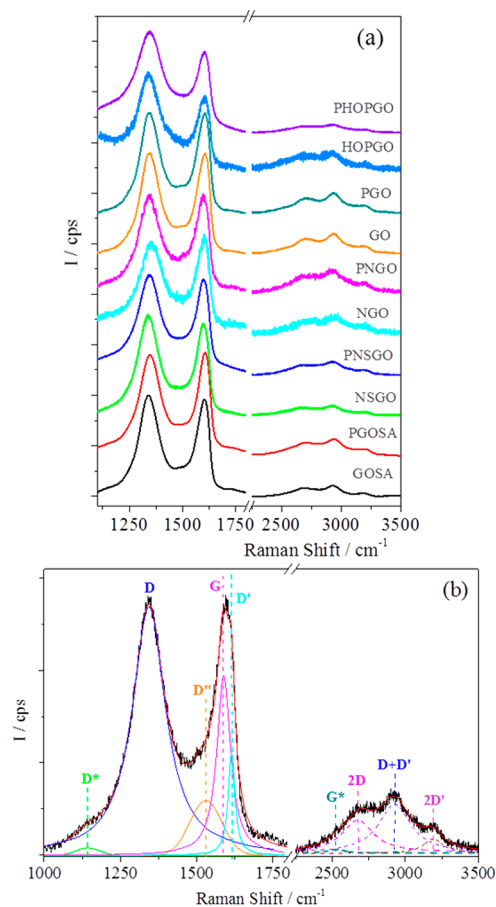


Figure 3. (a) Raman spectra of graphene oxides. For the sake of clarity, spectra have been vertically displaced. (b) Deconvolution of the Raman spectrum of PHOPGO.

spectra also present a broad shoulder between the D and G peaks. This shoulder was previously reported for reduced graphene oxides synthesized from GANF carbon nanofibers and further reduced by a thermal procedure.³⁴ The shoulder was interpreted with a new peak,³⁴ D'' (~ 1500 – 1550 cm^{-1}), that has been reported for some carbon-based materials.^{23,44,49–52} Our results confirmed that D'' is related to amorphous phases³⁴ because its intensity decreases when the crystallinity increases.⁵⁰ Another band, referred to as D^* (~ 1150 – 1200 cm^{-1}), was used to interpret the shoulder³⁴ observed below 1200 cm^{-1} . The D^* band was previously

reported and related to disordered graphitic lattices provided by sp^2 – sp^3 bonds.^{18,44}

In addition to these bands, other defect-related features such as D' and D + D' bands can be clearly observed in all of the spectra. In summary, the Raman spectra of graphene oxides synthesized from different starting materials were properly interpreted by fitting the first-order spectrum to five functions ascribed to D, G, D', D'', and D* bands. An illustrative example is provided in Figure 3b. The spectrum in Figure 3b corresponds to purified graphene oxide synthesized by the oxidation of highly oriented pyrolytic graphite (PHOPGO), but similar spectra were recorded for the rest of the graphene oxides (see Figure S3 on the section 2 of the Supporting Information). Table S1 of the Supporting Information collects the band parameters obtained from the fits.

The second-order spectrum was fitted to four Lorentzian functions. Figure 3b presents an illustrative example corresponding to the Raman spectrum of PHOPGO, and Figure S3 of the Supporting Information presents details of fittings for the rest of the Raman spectra. Table S2 of the Supporting Information collects the band parameters obtained from the fits. Our results showed very good agreement between the experimental spectrum and that calculated as a sum of the proposed functions.

To assign controversial spectral features in the second-order region of the spectra of the graphene oxides, we analyzed the bands appearing at about 2690 cm^{-1} (2D band), 2930 cm^{-1} (combination band), and 3190 cm^{-1} (overtone band). Toward this end, we have plotted the frequency of the 2D band against twice the frequency of the D band in Figure 4. Our results

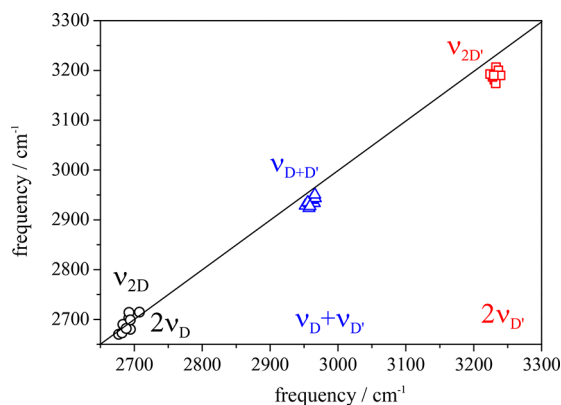


Figure 4. Frequencies of the second-order Raman spectra of graphene oxides, ν_{2D} , $\nu_{D+D'}$, and $\nu_{2D'}$, as functions of twice the frequency of the D band, the sum of frequencies of the D and D' bands, and twice the frequency of the D' band. For comparison the solid line represents the function $y = x$.

confirm that this band corresponds to the overtone of the D band. Similar analyses were performed for the D + D' and 2D' bands. In the former, the frequency of the D + D' band was plotted against the sum of frequencies of the D and D' bands, whereas for the 2D' band, its frequency was plotted against twice the frequency of the D' band. As can be seen in Figure 4, our data are in good agreement, confirming that these bands can be unambiguously assigned to D + D' and 2D', respectively.

The 2D and 2D' bands originate from processes in which momentum conservation is satisfied by two photon with opposite wave vectors and are always present in the spectrum

because they do not require defects for activation. In contrast, the D + D' band is the combination of phonons with different momenta and therefore, requires defects for its activation. In an attempt to analyze the effects of chemical composition on these bands, in Figure 5a, we present the positions of the bands against the Csp^2 percentage. As can be seen in Figure 5a, the band positions of both the 2D and D + D' bands correlate adequately with the Csp^2 percentage.

It has been well-established that the 2D band is related to the number of layers of graphene sheets and their relative orientations.²¹ For graphene monolayers, the 2D band was interpreted as a single Lorentzian with a full width at half-maximum (fwhm) of about 24 cm^{-1} , whereas when the number of layers increases, the 2D band can be decomposed into several Lorentzian peaks. However, in the particular case of turbostratic graphite in which the stacking of graphene monolayers is rotationally random with respect to one another, the 2D band is a single peak, just as for graphene but much wider. This behavior was attributed to the absence of interlayer interactions between graphene planes. In our graphene oxides obtained by the oxidation method previously reported by our group, the number of stacked layers is about two to three,^{10,35} therefore, we expected that the 2D band was not a single Lorentzian peak. On the contrary, we observed that, in all of the spectra, the 2D bands were broader single peaks. This fact allows for the conclusion that, in our graphene oxides, the different planes could be randomly oriented with a stacking order similar to that corresponding to turbostratic graphite.

As can be seen in Figure 3b, all of the Raman spectra present a weak band at about 2500 cm^{-1} . This peak, called the G* band, was previously reported and was explained using double-resonance theory with an intervalley process involving an in-plane transverse optical (iTO) phonon and one longitudinal acoustic (LA) phonon.⁵³ When we analyzed the position of the maximum of the G* peak (see Table S2 of the Supporting Information), we observed that the band position remained constant at $(2499 \pm 3) \text{cm}^{-1}$ in the case of the nonpurified samples, whereas it remained almost constant at a value of $(2536 \pm 9) \text{cm}^{-1}$ for the purified materials.

It is well-established that the relative intensity ratio of the D and G bands (I_D/I_G) is a good parameter for estimating the degree of graphitization of carbonaceous materials, as it is normally used for measuring the amount of defects. However, in the Raman spectrum of graphene oxide, the presence of the D'' and D* bands influences not only the relative intensity ratio I_D/I_G but also its position and fwhm. To eliminate these contributions, we calculated the relative intensity of the D and G bands considering the values after fitting the first-order spectrum to five functions; this ratio is referred to as $(I_D/I_G)_F$ hereafter. The $(I_D/I_G)_F$ values are collected in Table S3 of the Supporting Information and are plotted against the Csp^2 percentage of graphene oxide calculated from XPS measurements in Figure 5a. For the sake of comparison, the value corresponding to graphite is plotted in Figure 5a at the Csp^2 percentage of 100%.

As can be seen in Figure 5a, the $(I_D/I_G)_F$ values are higher than that corresponding to graphite and correlate very well with the Csp^2 percentage. Moreover, the positions of the maxima of the 2D and D + D' bands correlate adequately with the Csp^2 percentage (Figure 5b). Therefore, the $(I_D/I_G)_F$ value and the maximum positions of the 2D and D + D' bands could be used as good parameters for estimating the Csp^2 percentages of graphene oxide sheets. We checked the validity of these

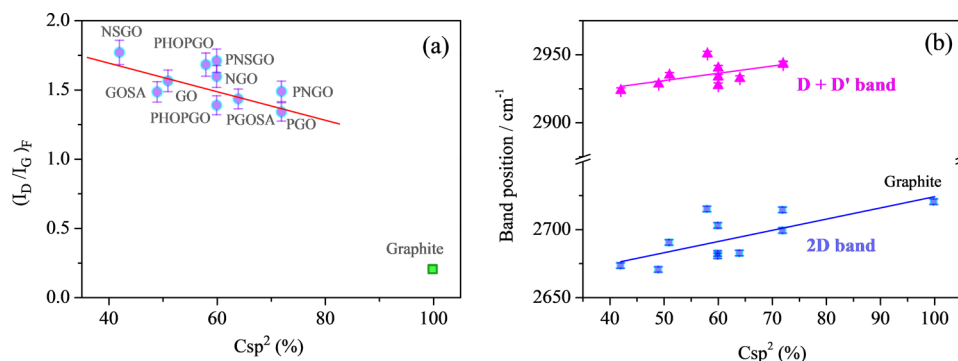


Figure 5. (a) Variations and relative intensities of the D and G bands obtained after the fit of the Raman spectra to the presented functions and (b) maximum positions of the 2D and D + D' bands as functions of the C_{sp^2} percentage. Solid lines correspond to linear fits of the experimental data.

correlations by calculating the C_{sp^2} percentages using the three correlations and comparing the results with those obtained from XPS measurements (see the details in section 3 of the [Supporting Information](#)). The results show that the C_{sp^2} percentages obtained from the three correlations agree with each other within the experimental margin of error and are consistent with the C_{sp^2} percentage values calculated from XPS measurements; see Figure S4 of the [Supporting Information](#). Therefore, the correlations reported in this work can be used to estimate the C_{sp^2} percentages of graphene oxides.

Regarding the D^* and D'' bands, in a previous work,³⁴ we found that the positions of the maxima of the D^* and D'' bands depend on the oxygen content determined by chemical analysis. Specifically, the maximum of the D^* band was shifted to shorter wavelength when the oxygen content increased, whereas the maximum position of the D'' band was shifted to longer wavelengths until an oxygen content of about 20%, after which the band positions remained constant at 1125 and 1526 cm^{-1} , respectively. Our current results agree very well with that behavior because the oxygen contents of the graphene oxides synthesized in this work from distinct starting materials and calculated from XPS were greater than 22% and the band positions remained almost constant at (1124 ± 32) and (1521 ± 12) cm^{-1} for the D^* and D'' bands, respectively.

On the other hand, in our previous work,³⁴ we also confirmed that the I_{D^*}/I_G ratio correlates very well with the oxygen content.³⁴ In that work, we reported a sigmoid dependence between the I_{D^*}/I_G ratio and the oxygen content. Specifically, the I_{D^*}/I_G ratio increased when the oxygen content increased until it reached a constant value of 0.15 at an oxygen percentage of 20%. The I_{D^*}/I_G ratios found for our graphene oxides agree very well with the previous results, because the oxygen contents of our graphene oxides were greater than 22% and the I_{D^*}/I_G values remained constant for the different materials at 0.15 ± 0.02 . Accordingly, the results presented in the current work are in good agreement with the correlations previously reported for thermally reduced graphene oxides.³⁴

The D' peak has been reported for graphene with defects generated by Ar^+ ion bombardment,^{27,54} plasma treatment,⁵⁵ and anodic bonding,⁵⁶ as well as for graphite⁵⁷ and carbon nanotubes subjected to mechanical stress, and ascribed to highly defective layers. Moreover, from the evolution of the intensities of the D' and D bands, it is possible to identify the types of defects in the graphene sheets.⁵⁷ Therefore, we analyzed the evolution of the intensities of the D' and D bands of our Raman spectra to obtain information about the types of defects in the graphene oxides. To the best of our knowledge,

this is the first time that this treatment has been applied to the Raman spectra of graphene oxides.

To interpret the evolution of the D' band with structural defects, we used the double-resonance mechanism for defective graphene.⁵⁹ According to this mechanism, an increase in the number of defects affects the electron lifetime, decreasing the band intensities. This is valid for the D and D' bands, as well as for the 2D band; moreover, the intensities of D and D' bands are also proportional to the defect concentration and to the types of defects, grain boundaries, vacancies, or sp^3 hybridization.⁵⁹ Consequently, for graphene oxides, we expect that the presence of C_{sp^3} and structural defects produced during oxidation could be responsible for the presence of the D' band in their Raman spectra. Therefore, we analyzed the relationship between the intensities of the D' and D bands for our graphene oxides. Previously, it was necessary to take into account the terminology introduced by Ferrari et al. for the interpretation of the Raman spectra of disordered graphene. These authors demonstrated that the I_D/I_G ratio follows a two-stage evolution:¹⁷ Stage 1 corresponds to low-defect graphene, and stage 2 corresponds to disordered graphene. They established the transition between stages 1 and 2 at I_D/I_G values of about 3.5, at 2.41 eV for a mean distance between two defects (L_d) of 3–5 nm. This value was recently confirmed for graphene samples with different types of defects.^{54,55} They also demonstrated that, in stage 1, the intensities of both the D and D' peaks are proportional to the defect concentration; as a consequence, they are proportional to each other. However, in stage 2, the effect of the electron lifetime predominates, and the relationship between the intensities of the D and D' bands becomes more complicated than that in stage 1. In our materials, the I_D/I_G values are less than 3.5; therefore, we expect that they present low defect degrees, or stage 1. To differentiate between stages 1 and 2, we plot in [Figure 6](#) the relative intensity expressed as the integrated area of the D' band, $A_{D'}/A_G$, against the relative intensity of the D band, A_D/A_G . In this treatment the ratio of the integrated areas instead the intensity is preferred⁵⁴ because the area under the band represents the probability of the whole scattering process. The relative area values are collected in Table S3 of the [Supporting Information](#). As can be seen in [Figure 6](#), our results show two different trends.

To analyze the two trends observed, the data in [Figure 6](#) were fitted to value found for the $A_{D'}/A_D$ ratio. Two different $A_{D'}/A_D$ values of 0.145 and 0.076 were found. We compared our values with those obtained from ab initio calculations used to simulate the Raman spectra of graphene with specific defects.

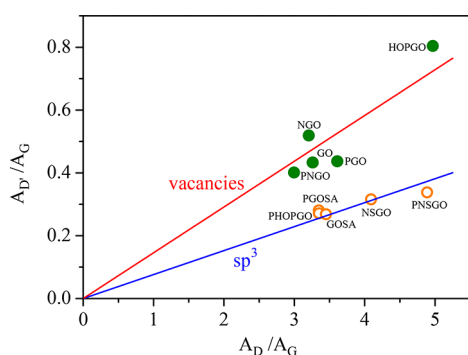


Figure 6. Variation in the relative intensity of the D' band in terms of integrated area with the relative intensity of the D band for different graphene oxides. Solid lines correspond to linear fits of the experimental data.

The calculations showed that defective graphene at stage 1 containing vacancies is characterized by an $A_{D'}/A_D$ value of 0.143, whereas graphene with sp^3 defects presents an $A_{D'}/A_D$ value of 0.077.^{55,57,59} The $A_{D'}/A_D$ values found in this work are in excellent agreement with theoretical values, indicating that two types of defects predominate in our graphene oxides: vacancies and sp^3 defects. Moreover, our results show that materials in which vacancy-like defects predominate correspond to the largest graphene oxide sheets ($D_{app} > 400$ nm), whereas those with defects associated with sp^3 hybridization correspond to the smallest sheets, $D_{app} \approx 100$ nm. Consequently, our results seem to indicate that vacancies are favored in the largest sheets. This behavior could be due to the fact that the high surface areas of larger sheets favor the formation of vacancies in the network during chemical oxidation.

4. CONCLUSIONS

We have synthesized 10 different graphene oxides by the oxidation of five distinct starting materials and subsequent purification of these oxides. The nanoplatelet characterization by XPS, ζ -potential, and dynamic light scattering (DLS) measurements demonstrated that the chemical composition, superficial charge density, and nanoplatelet size can be modified by combining the chemical oxidation of different starting materials with purification by alkaline washing. The Raman spectra of the graphene oxides were analyzed by fitting the first-order Raman spectra of different graphene oxides to five Raman bands (D, D', G, D'', and D*) previously reported for thermally reduced graphene oxide.³⁴ We also analyzed the second-order spectra of the graphene oxides and noticed the presence of three intense peaks assigned to the 2D, 2D', and D + D' bands. We demonstrated that the relative intensity of the D band with respect to the G peak and the maximum positions of the 2D and D + D' bands linearly correlate with the C_{sp^2} percentage and can be used to evaluate the C_{sp^2} percentages of graphene oxides.

Finally, we found that the relative intensities expressed as the integrated areas of the defective D and D' bands are strongly correlated, and from the $A_{D'}/A_D$ values, we demonstrated that, in large graphene oxide sheets ($D_{app} > 400$ nm), vacancy-like defects predominate, whereas defects associated with sp^3 hybridization predominate in the smallest sheets, $D_{app} \approx 100$ nm. Consequently, the correlations between the areas of the D' and D bands reported in this work allow the nature of the defects in graphene oxides to be differentiated.

■ ASSOCIATED CONTENT

Supporting Information

The Supporting Information is available free of charge on the ACS Publications website at DOI: 10.1021/acs.jpcc.7b06236.

XPS spectra of different graphene oxides, size distribution functions obtained by dynamic light scattering of graphene oxide nanoplatelets, deconvolution of first- and second-order Raman spectra and parameters calculated from fits, and Raman correlations for estimating the C_{sp^2} percentages of graphene oxides (PDF)

■ AUTHOR INFORMATION

Corresponding Author

*E-mail: mvsal@usal.es.

ORCID

M. Mercedes Velázquez: 0000-0003-2746-8204

Notes

The authors declare no competing financial interest.

■ ACKNOWLEDGMENTS

We acknowledge financial support from European Regional Development Fund (ERDF), Junta de Castilla y León (SA045U16) and MINECO (CTQ2016-78895-R, UNSA13-3E-2302). The authors also thank Prof. V.G. Baonza for helpful discussions.

■ ABBREVIATIONS

- GO = graphene oxide synthesized by oxidation of natural graphite flakes
- GOSA = graphene oxide synthesized by oxidation of graphite flakes (+100 mesh)
- HOPGO = graphene oxide synthesized by oxidation of highly oriented pyrolytic graphite
- NGO = graphene oxide synthesized by oxidation of GANF carbon nanofibers (graphitized)
- NSGO = graphene oxide synthesized by oxidation of GANF carbon nanofibers (nongraphitized)
- PGO = purified graphene oxide synthesized by oxidation of natural graphite flakes
- PGOSA = purified graphene oxide synthesized by oxidation of graphite flakes (+100 mesh)
- PHOPGO = purified graphene oxide synthesized by oxidation of highly oriented pyrolytic graphite
- PNGO = purified graphene oxide synthesized by oxidation of GANF carbon nanofibers (graphitized)
- PNSGO = purified graphene oxide synthesized by oxidation of GANF carbon nanofibers (nongraphitized)

■ REFERENCES

- (1) Geim, A. K.; Novoselov, K. S. The Rise of Graphene. *Nat. Mater.* **2007**, *6*, 183–91.
- (2) Lee, C.; Wei, X.; Kysar, J. W.; Hone, J. Measurement of the Elastic Properties and Intrinsic Strength of Monolayer Graphene. *Science* **2008**, *321*, 385–388.
- (3) Edwards, R. S.; Coleman, K. S. Graphene Synthesis: Relationship to Applications. *Nanoscale* **2013**, *5*, 38–51.
- (4) Obratzsov, A. N. Chemical Vapour Deposition: Making Graphene on a Large Scale. *Nat. Nanotechnol.* **2009**, *4*, 212–3.
- (5) Sutter, P. Epitaxial Graphene: How Silicon Leaves the Scene. *Nat. Mater.* **2009**, *8*, 171–172.
- (6) Subrahmanyam, K. S.; Vivekchand, S. R. C.; Govindaraj, A.; Rao, C. N. R. A Study of Graphenes Prepared by Different Methods:

Characterization, Properties and Solubilization. *J. Mater. Chem.* **2008**, *18*, 1517–1523.

(7) Yoon, G.; Seo, D.-H.; Ku, K.; Kim, J.; Jeon, S.; Kang, K. Factors Affecting the Exfoliation of Graphite Intercalation Compounds for Graphene Synthesis. *Chem. Mater.* **2015**, *27*, 2067–2073.

(8) Hummers, W. S.; Offeman, R. E. Preparation of Graphitic Oxide. *J. Am. Chem. Soc.* **1958**, *80*, 1339–1339.

(9) Pei, S.; Cheng, H.-M. The Reduction of Graphene Oxide. *Carbon* **2012**, *50*, 3210–3228.

(10) Martín-García, B.; Velázquez, M. M.; Rossella, F.; Bellani, V.; Diez, E.; García Fierro, J. L.; Pérez-Hernández, J. A.; Hernández-Toro, J.; Claramunt, S.; Cirera, A. Functionalization of Reduced Graphite Oxide Sheets with a Zwitterionic Surfactant. *ChemPhysChem* **2012**, *13*, 3682–3690.

(11) Stankovich, S.; Dikin, D. A.; Piner, R. D.; Kohlhaas, K. A.; Kleinhammes, A.; Jia, Y.; Wu, Y.; Nguyen, S. T.; Ruoff, R. S. Synthesis of Graphene-Based Nanosheets Via Chemical Reduction of Exfoliated Graphite Oxide. *Carbon* **2007**, *45*, 1558–1565.

(12) Thomas, H. R.; Day, S. P.; Woodruff, W. E.; Vallés, C.; Young, R. J.; Kinloch, I. A.; Morley, G. W.; Hanna, J. V.; Wilson, N. R.; Rourke, J. P. Deoxygenation of Graphene Oxide: Reduction or Cleaning? *Chem. Mater.* **2013**, *25*, 3580–3588.

(13) Potts, J. R.; Dreyer, D. R.; Bielawski, C. W.; Ruoff, R. S. Graphene-Based Polymer Nanocomposites. *Polymer* **2011**, *52*, 5–25.

(14) Prezioso, S.; Perrozzi, F.; Giancaterini, L.; Cantalini, C.; Treossi, E.; Palermo, V.; Nardone, M.; Santucci, S.; Ottaviano, L. Graphene Oxide as a Practical Solution to High Sensitivity Gas Sensing. *J. Phys. Chem. C* **2013**, *117*, 10683–10690.

(15) Eda, G.; Chhowalla, M. Chemically Derived Graphene Oxide: Towards Large-Area Thin-Film Electronics and Optoelectronics. *Adv. Mater.* **2010**, *22*, 2392–2415.

(16) Loh, K. P.; Bao, Q.; Eda, G.; Chhowalla, M. Graphene Oxide as a Chemically Tunable Platform for Optical Applications. *Nat. Chem.* **2010**, *2*, 1015–1024.

(17) Ferrari, A. C.; Robertson, J. Interpretation of Raman Spectra of Disordered and Amorphous Carbon. *Phys. Rev. B: Condens. Matter Mater. Phys.* **2000**, *61*, 14095–14107.

(18) Ferrari, A. C.; Robertson, J. Resonant Raman Spectroscopy of Disordered, Amorphous, and Diamondlike Carbon. *Phys. Rev. B: Condens. Matter Mater. Phys.* **2001**, *64*, 075414.

(19) Ferrari, A. C.; Meyer, J. C.; Scardaci, V.; Casiraghi, C.; Lazzeri, M.; Mauri, F.; Piscanec, S.; Jiang, D.; Novoselov, K. S.; Roth, S.; Geim, A. K. Raman Spectrum of Graphene and Graphene Layers. *Phys. Rev. Lett.* **2006**, *97*, 187401.

(20) Pimenta, M. A.; Dresselhaus, G.; Dresselhaus, M. S.; Cancado, L. G.; Jorio, A.; Saito, R. Studying Disorder in Graphite-Based Systems by Raman Spectroscopy. *Phys. Chem. Chem. Phys.* **2007**, *9*, 1276–91.

(21) Malard, L. M.; Pimenta, M. A.; Dresselhaus, G.; Dresselhaus, M. S. Raman Spectroscopy in Graphene. *Phys. Rep.* **2009**, *473*, 51–87.

(22) Jia, X.; Campos-Delgado, J.; Terrones, M.; Meunier, V.; Dresselhaus, M. S. Graphene Edges: A Review of Their Fabrication and Characterization. *Nanoscale* **2011**, *3*, 86–95.

(23) Saito, R.; Hofmann, M.; Dresselhaus, G.; Jorio, A.; Dresselhaus, M. S. Raman Spectroscopy of Graphene and Carbon Nanotubes. *Adv. Phys.* **2011**, *60*, 413–550.

(24) Jorio, A.; Saito, R.; Dresselhaus, G.; Dresselhaus, M. S. *Raman Spectroscopy in Graphene Related Systems*; Wiley-VCH Verlag GmbH & Co.: Weinheim, Germany, 2011.

(25) Tuinstra, F.; Koenig, J. L. Raman Spectrum of Graphite. *J. Chem. Phys.* **1970**, *53*, 1126–1130.

(26) Cançado, L. G.; Jorio, A.; Ferreira, E. H. M.; Stavale, F.; Achete, C. A.; Capaz, R. B.; Moutinho, M. V. O.; Lombardo, A.; Kulmala, T. S.; Ferrari, A. C. Quantifying Defects in Graphene Via Raman Spectroscopy at Different Excitation Energies. *Nano Lett.* **2011**, *11*, 3190–3196.

(27) Martins Ferreira, E. H.; Moutinho, M. V. O.; Stavale, F.; Lucchese, M. M.; Capaz, R. B.; Achete, C. A.; Jorio, A. Evolution of the Raman Spectra from Single-, Few-, and Many-Layer Graphene with

Increasing Disorder. *Phys. Rev. B: Condens. Matter Mater. Phys.* **2010**, *82*, 125429.

(28) Kaniyoor, A.; Ramaprabhu, S. A Raman Spectroscopic Investigation of Graphite Oxide Derived Graphene. *AIP Adv.* **2012**, *2*, 032183–13.

(29) King, A. A. K.; Davies, B. R.; Noorbehesht, N.; Newman, P.; Church, T. L.; Harris, A. T.; Razal, J. M.; Minett, A. I. A New Raman Metric for the Characterisation of Graphene Oxide and Its Derivatives. *Sci. Rep.* **2016**, *6*, 19491.

(30) Szabó, T.; Berkesi, O.; Forgó, P.; Josepovits, K.; Sanakis, Y.; Petridis, D.; Dékány, I. Evolution of Surface Functional Groups in a Series of Progressively Oxidized Graphite Oxides. *Chem. Mater.* **2006**, *18*, 2740–2749.

(31) Diez-Betriu, X.; Alvarez-Garcia, S.; Botas, C.; Alvarez, P.; Sanchez-Marcos, J.; Prieto, C.; Menendez, R.; de Andres, A. Raman Spectroscopy for the Study of Reduction Mechanisms and Optimization of Conductivity in Graphene Oxide Thin Films. *J. Mater. Chem. C* **2013**, *1*, 6905–6912.

(32) Wang, L.; Zhao, J.; Sun, Y.-Y.; Zhang, S. B. Characteristics of Raman Spectra for Graphene Oxide from Ab Initio Simulations. *J. Chem. Phys.* **2011**, *135*, 184503.

(33) Kudin, K. N.; Ozbas, B.; Schniepp, H. C.; Prud'homme, R. K.; Aksay, I. A.; Car, R. Raman Spectra of Graphite Oxide and Functionalized Graphene Sheets. *Nano Lett.* **2008**, *8*, 36–41.

(34) Claramunt, S.; Varea, A.; López-Díaz, D.; Velázquez, M. M.; Cornet, A.; Cirera, A. The Importance of Interbands on the Interpretation of the Raman Spectrum of Graphene Oxide. *J. Phys. Chem. C* **2015**, *119*, 10123–10129.

(35) López-Díaz, D.; Mercedes Velázquez, M.; Blanco de La Torre, S.; Pérez-Pisonero, A.; Trujillano, R.; Fierro, J. L. G.; Claramunt, S.; Cirera, A. The Role of Oxidative Debris on Graphene Oxide Films. *ChemPhysChem* **2013**, *14*, 4002–4009.

(36) Orna, J.; López-Díaz, D.; Pérez, A.; Rodríguez, M. J.; Lagunas, A. R.; Velázquez, M. M.; Blanco, S.; Merino, C. GRANPH®: High Quality Graphene Oxide Obtained from GANF® Carbon Nanofibres. *eNanoneletter* **2013**, No. 27, 33–37.

(37) Blake, P.; Hill, E. W.; Castro Neto, A. H.; Novoselov, K. S.; Jiang, D.; Yang, R.; Booth, T. J.; Geim, A. K. Making Graphene Visible. *Appl. Phys. Lett.* **2007**, *91*, 063124–3.

(38) Rourke, J. P.; Pandey, P. A.; Moore, J. J.; Bates, M.; Kinloch, I. A.; Young, R. J.; Wilson, N. R. The Real Graphene Oxide Revealed: Stripping the Oxidative Debris from the Graphene-Like Sheets. *Angew. Chem., Int. Ed.* **2011**, *50*, 3173–3177.

(39) Hidalgo, R. S.; López-Díaz, D.; Mercedes Velázquez, M. Graphene Oxide Thin Films: Influence of Chemical Structure and Deposition Methodology. *Langmuir* **2015**, *31*, 2697–2705.

(40) Mercedes Velázquez, M.; Alejo, T.; López-Díaz, D.; Martín-García, B.; Merchán, M. D., Langmuir-Blodgett Methodology: A Versatile Technique to Build 2D Material Films. In *Two-Dimensional Materials - Synthesis, Characterization and Potential Applications*; Nayak, P. K., Ed.; InTech: Rijeka, Croatia, 2016; Chapter 2, pp 21–42.

(41) Smoluchowski, M. v. Elektrische Endosmose und Strömungsströme. In *Handbuch der Elektrizität und des Magnetismus*; Graetz, L., Ed.; Barth: Leipzig, Germany, 1921; Vol. II.

(42) Pecora, R. Doppler Shifts in Light Scattering from Pure Liquids and Polymer Solutions. *J. Chem. Phys.* **1964**, *40*, 1604–1614.

(43) Zickler, G. A.; Smarsly, B.; Gierlinger, N.; Peterlik, H.; Paris, O. A Reconsideration of the Relationship between the Crystallite Size La of Carbons Determined by X-Ray Diffraction and Raman Spectroscopy. *Carbon* **2006**, *44*, 3239–3246.

(44) Sadezky, A.; Muckenhuber, H.; Grothe, H.; Niessner, R.; Pöschl, U. Raman Microspectroscopy of Soot and Related Carbonaceous Materials: Spectral Analysis and Structural Information. *Carbon* **2005**, *43*, 1731–1742.

(45) Paris, O.; Zollfrank, C.; Zickler, G. A. Decomposition and Carbonisation of Wood Biopolymers—a Microstructural Study of Softwood Pyrolysis. *Carbon* **2005**, *43*, 53–66.

(46) Yamauchi, S.; Kurimoto, Y. Raman Spectroscopic Study on Pyrolyzed Wood and Bark of Japanese Cedar: Temperature Dependence of Raman Parameters. *J. Wood Sci.* **2003**, *49*, 235–240.

(47) Hontoria-Lucas, C.; López-Peinado, A. J.; López-González, J. d. D.; Rojas-Cervantes, M. L.; Martín-Aranda, R. M. Study of Oxygen-Containing Groups in a Series of Graphite Oxides: Physical and Chemical Characterization. *Carbon* **1995**, *33*, 1585–1592.

(48) Matsubara, I.; Hosono, K.; Murayama, N.; Shin, W.; Izu, N. Organically Hybridized SnO₂ Gas Sensors. *Sens. Actuators, B* **2005**, *108*, 143–147.

(49) Goodman, P. A.; Li, H.; Gao, Y.; Lu, Y. F.; Stenger-Smith, J. D.; Redepenning, J. Preparation and Characterization of High Surface Area, High Porosity Carbon Monoliths from Pyrolyzed Bovine Bone and Their Performance as Supercapacitor Electrodes. *Carbon* **2013**, *55*, 291–298.

(50) Vollebregt, S.; Ishihara, R.; Tichelaar, F. D.; Hou, Y.; Beenakker, C. I. M. Influence of the Growth Temperature on the First and Second-Order Raman Band Ratios and Widths of Carbon Nanotubes and Fibers. *Carbon* **2012**, *50*, 3542–3554.

(51) Jawhari, T.; Roid, A.; Casado, J. Raman Spectroscopic Characterization of Some Commercially Available Carbon Black Materials. *Carbon* **1995**, *33*, 1561–1565.

(52) Nemanich, R. J.; Solin, S. A. First- and Second-Order Raman Scattering from Finite-Size Crystals of Graphite. *Phys. Rev. B: Condens. Matter Mater. Phys.* **1979**, *20*, 392–401.

(53) Maultzech, J.; Reich, S.; Thomsen, C. Double-Resonant Raman Scattering in Graphite: Interference Effects, Selection Rules, and Phonon Dispersion. *Phys. Rev. B: Condens. Matter Mater. Phys.* **2004**, *70*, 155403.

(54) Lucchese, M. M.; Stavale, F.; Ferreira, E. H. M.; Vilani, C.; Moutinho, M. V. O.; Capaz, R. B.; Achete, C. A.; Jorio, A. Quantifying Ion-Induced Defects and Raman Relaxation Length in Graphene. *Carbon* **2010**, *48*, 1592–1597.

(55) Eckmann, A.; Felten, A.; Mishchenko, A.; Britnell, L.; Krupke, R.; Novoselov, K. S.; Casiraghi, C. Probing the Nature of Defects in Graphene by Raman Spectroscopy. *Nano Lett.* **2012**, *12*, 3925–3930.

(56) Moldt, T.; Eckmann, A.; Klar, P.; Morozov, S. V.; Zhukov, A. A.; Novoselov, K. S.; Casiraghi, C. High-Yield Production and Transfer of Graphene Flakes Obtained by Anodic Bonding. *ACS Nano* **2011**, *5*, 7700–7706.

(57) del Corro, E.; Taravillo, M.; Baonza, V. G. Stress-Dependent Correlations for Resonant Raman Bands in Graphite with Defects. *J. Raman Spectrosc.* **2014**, *45*, 476–480.

(58) del Corro, E.; Taravillo, M.; González, J.; Baonza, V. G. Raman Characterization of Carbon Materials under Non-Hydrostatic Conditions. *Carbon* **2011**, *49*, 973–979.

(59) Venezuela, P.; Lazzeri, M.; Mauri, F. Theory of Double-Resonant Raman Spectra in Graphene: Intensity and Line Shape of Defect-Induced and Two-Phonon Bands. *Phys. Rev. B: Condens. Matter Mater. Phys.* **2011**, *84*, 035433.